Force production by a bundle of growing actin filaments is limited by its mechanical properties

Jean-Louis Martiel, Alphee Michelot, Rajaa Boujemaa-Paterski, Laurent Blanchoin, Julien Berro

Force production by a bundle of growing actin filaments is limited by its mechanical properties

Authors: Jean-Louis Martiel[1,2*], Alphée Michelot[1,3], Rajaa Boujemaa-Paterski[1,4], Laurent Blanchoin[1], Julien Berro[1,5,6,7*]

Affiliations:
[1] CytomorphoLab, Biosciences & Biotechnology Institute of Grenoble, Laboratoire de Physiologie Cellulaire & Végétale, Université Grenoble-Alpes/CEA/CNRS/INRA, Grenoble, France.
[2] Univ. Grenoble-Alpes, CNRS, CHU Grenoble Alpes, Inserm, TIMC-IMAG, F-38000 Grenoble, France.
[3] Aix Marseille Univ, CNRS, IBDM, Turing Centre for Living Systems, Marseille, France
[4] Department of Biochemistry, University of Zurich, Winterthurerstrasse 190, 8057 Zurich, Switzerland.
[5] Department of Molecular Biophysics and Biochemistry, Yale University, New Haven, CT 06520, USA.
[6] Nanobiology Institute, Yale University, West Haven, CT 06516, USA.
[7] Department of Cell Biology, Yale University School of Medicine, New Haven, CT, 06520, USA.

*Corresponding authors e-mail:Jean-Louis.Martiel@univ-grenoble-alpes.fr , julien.berro@yale.edu

ABSTRACT

Bundles of actin filaments are central to a large variety of cellular structures, such as filopodia, stress fibers, cytokinetic rings or focal adhesions. The mechanical properties of these bundles are critical for proper force transmission and force bearing. Previous mathematical modeling efforts have focused on bundles' rigidity and shape. However, it remains unknown how bundle length and buckling are controlled by external physical factors. In this paper, we present a biophysical model for dynamic bundles of actin filaments submitted to an external load. In combination with *in vitro* motility assays of beads coated with formins, our model allowed us to characterize conditions for bead movement and bundle buckling. From the deformation profiles, we determined key biophysical properties of tethered actin bundles, such as their rigidity and filament density.

STATEMENT OF SIGNIFICANCE

Groups of dynamic and parallel actin filaments, called bundles, can produce and sustain more force than isolated filaments. In this paper, we perform experiments where bundles of filaments grow from micrometric beads with their dynamic ends facing the load. We show that a straight bundle can steadily push the bead forward, until the bundle becomes too long and bends, stopping the motion of the bead. We develop a mathematical model that recapitulates this behavior, explains the balance of the forces involved, and identifies the conditions under which movement is possible.

INTRODUCTION

Bundles of actin filaments are involved in a large variety of cellular structures, such as filopodia (1), the cytokinetic ring (2, 3), auditory hair cells (4), actin cables (5, 6), stress fibers (7, 8), focal adhesions (9), adherens junction (10), and are hijacked by some pathogens for their propulsion within and between host cells (11). Bundles also determine the shape of macroscopic structures like Drosophila bristles (12) and are the core of microvilli (13, 14).

In motile cells, bundles of actin filaments can develop large amounts of force that deform the cell membrane at the leading edge (13, 15, 16), and are used to generate tension in stress fibers (17). Filopodial bundles are created by formin- and Ena/Vasp- mediated assembly of parallel actin filaments. In the lamella, actin filaments from the lamellipodium are condensed into bundles under the action of the retrograde flow and motor proteins. Through these bundles, cells optimize and adapt their response to mechanical stress and disassemble the actin cytoskeleton at their trailing edge (18–20).

A limiting factor for force production is filament buckling (20–22). Buckling occurs when the force exerted between the ends of the filament reaches a critical value, which depends on the mechanical properties of the filament, its geometry, and the attachment conditions of its ends (23, 24). When buckling occurs the force produced by a filament (or a bundle) vanishes.

Theoretical and *in vitro* biophysical studies have determined the mechanical properties of bundles of actin filaments (15, 25, 26), and analyzed the effects of crosslinkers (27), motor proteins (21, 22, 28), active transport (29), or combinations thereof to mimic constricting cytokinetic rings (21, 30–34). These studies essentially focused on the effect of bundle rigidity on its stability and shape, and how filament dynamics and membrane tension control the bundle length. In particular, a careful analysis of the physics of protrusion determined the optimal number of filament in a filopodium and its length (15). These quantitative predictions represents the first attempt to understand the dynamics of filopodia and classify their morphology (length, number of filaments in the bundle or inter-filopodium distance). However, despite these experimental and theoretical studies, it remains unknown how bundle length and buckling are controlled by external physical factors.

In this paper, we present a biophysical model for bundles of dynamic actin filaments. The model is supported by experimental *in vitro* reconstitution of bead motility powered by bundles of actin filaments, which are nucleated on the bead surface by formins. Here, formins also play the role of tethers that maintain filament barbed ends on the bead. Using our experimental data we quantified the bead movement and correlated it with the elongation and deformation of filament bundles. This allowed us to determine bundle's rigidity and average number of filaments. Thus, using these two experimentally-measured constraints, we propose an original, simple and robust model for the movement and deformation of actin filaments that predicts how filament mechanics tunes the force that can be produced by dynamic actin filament bundles.

MATERIALS AND METHODS

Experimental data

Motility assay

Experiments performed in this study were carried out according to the procedure described in (35). In brief, beads grafted with the FH1-FH2 domains of mDia1 were mixed with a motility medium containing 8 μM F-actin, 4 μM profilin, and 10 μM human cofilin in X buffer (10 mM HEPES pH 7.8, 0.1 M KCl, 1 mM MgCl2, 1 mM ATP, and 0.1 mM CaCl2), supplemented with 1% BSA, 0.2% methylcellulose, 3 mM DTT, 1.8 mM ATP, and 0.1 mM DABCO.

Microscopy

Motility assays were acquired with a Zeiss Axioplan microscope (Jena, Germany) equipped with a 63x/1.5NA Plan-APOCHROMAT objective lens, a Hamamatsu ORCA CCD camera (Hamamatsu Photonics Deutschland GmbH) and Metavue version 6.2r6 (Universal Imaging, Media, PA).

Buckles of filaments were imaged using Total Internal Reflection Microscopy (TIRFM). Glass flow cells were cleaned and prepared according to (36). Rhodamine-actin and Alexa-532-labeled actin-filament polymerization was observed and acquired as specified in (37).

Theory and simulations

Mechanical equilibrium equations for an actin filament

We developed a model for the mechanical equilibrium of elastic filaments subjected to external forces and constraints based on a model we previously developed (38). In this section, we present the definitions of variables and the equations for force and moment balance. The orientation of the filament cross-section at any point along the filament is given by a set of three unit vectors $(\mathbf{d}_1, \mathbf{d}_2, \mathbf{d}_3)$ which define the material frame associated with position **r**(s) (Fig. S1A). The filament bending or twisting strain $\boldsymbol{\kappa}$, the density of force **f,** and moment **m** vectors are defined in the material frame as $\boldsymbol{\kappa} = \kappa_1\mathbf{d}_1 + \kappa_2\mathbf{d}_2 + \kappa_3\mathbf{d}_3$, $\mathbf{f} = f_1\mathbf{d}_1 + f_2\mathbf{d}_2 + f_3\mathbf{d}_3$, $\mathbf{m} = m_1\mathbf{d}_1 + m_2\mathbf{d}_2 + m\mathbf{d}_3$. The moment is proportional to the filament bending strains $\mathbf{m} = B\boldsymbol{\kappa}$ where *B* is the bending rigidities diagonal matrix (C_B, C_B, C_T) . The balance of force and moment reads

$$\begin{aligned} \frac{\partial \mathbf{f}}{\partial s} + \boldsymbol{\kappa} \times \mathbf{f} &= \mathbf{f}_{ext} \\ \frac{\partial \mathbf{m}}{\partial s} + \boldsymbol{\kappa} \times B\boldsymbol{\kappa} + \mathbf{d_3} \times \mathbf{f} &= \mathbf{m}_{ext} \end{aligned} \qquad Eq.\,1$$

where $\mathbf{f}_{ext}$ and $\mathbf{m}_{ext}$ are the external force and moment densities applied to the filament at position *s*. All filament-filament or filament-medium interactions are modeled by adapting the expression for $\mathbf{f}_{ext}$ in Eq. 1. The unit tangent vector, denoted $\mathbf{d}_3$, is given by

$$\frac{d\mathbf{r}}{ds} = \mathbf{d}_3 \qquad Eq.\,2$$

where **r** is a point along the filament (Fig. S1A). Since filaments move at low Reynolds number (~ 10^{-5}), all force and moment terms proportional to linear or angular acceleration were eliminated from Eq. 1 (38). The components of the material frame $(\mathbf{d}_1, \mathbf{d}_2, \mathbf{d}_3)$ vectors are parametrized by Euler parameters (unit quaternions), which couple the change of the cross section orientation to the force-moment applied at *s*.

In appendix A, we simplify this 3D model to develop a general method for the analysis of filaments or bundles of filaments considered as 2D elastic structures and the measurement of the polymerization and drag forces (Appendix A). In appendix B, we adapt this model to the analysis of bead movement.

RESULTS

Buckling of actin filament bundles limits the motility of formin-grafted beads

When placed in a motility medium containing actin monomers, profilin and cofilin (35, 39), beads coated with formin mDia1 nucleate actin filaments at their surface (Fig. 1A). These elongating filaments rapidly form long bundles of actin filaments, which propel the bead at a constant velocity about 0.25 $\mu m.min^{-1}$ for a duration that varied from a few minutes to over one hour, when the experiment was stopped (Fig. 2). In most cases, beads eventually stalled and remained permanently stuck to the coverslip (Figs. 1A and 2). During the motility phase, bead trajectories were rectilinear, their bundle remained straight (Fig.1A), and the bead velocity and the bundle elongation rate were identical (Fig. 2). After beads stalled, bundles continued growing at the same elongation rate while deforming to eventually form a large buckle (Fig. 3).

What is the cause of bead movement and why do beads stall? Since filaments in bundles grow at the same rate when beads are moving and when beads are stalled, we deduced that actin monomer concentration and viscosity of the motility medium remained constant (Fig. 2). In consequence, these two factors cannot account for the changes of the bead velocity. We hypothesized that the variety of motility behavior observed experimentally is due to the variations in the mechanical properties of the bundle of actin filaments over time.

Determination of bundle rigidity and depletion forces from loop geometries

To test our hypothesis, we took advantage of loops formed by long filaments (Fig. 3A, 3B and 3E) and bundles of filaments (Fig. 3F) at the end of our experiments. These loops are typical of semi-flexible polymers in a solvent and appear because depletion forces tend to bundle both ends of the filaments (40). Since we do not have enough movies with the full time course of the dynamical formation of these loops, we analyzed pictures of already formed, stable, bundle loops. We assumed that these loops are elastic structures at equilibrium, where the elastic bending force of the filament (or bundle) which tends to open the loop, and the attractive depletion forces that keep the stem of the loop closed, balanced each other (Fig. 3D, Appendix A, equations A1-A.2). To further simplify the analysis and simulations, we assume that the filaments in the bundle are intact (no internal gap) and run along the whole bundle length. In addition, in agreement with the experimental conditions, we assume that the filaments in the bundle remain independent and can slide without friction during the bundle deformation.

The persistence length of bundles can be directly deduced by fitting the shape of the loops to our model (equations A.5-A.6 and Figs. 3E, 3F, and 4A). As expected, the apparent persistence length of bundles increased with the number of formin molecules bound to the bead, and

plateaued at larger formin density, probably because friction between filaments becomes high, but is not accounted for in our model. (Figs. 4B, 4C and 4D). However, our results show that the number of filaments is significantly smaller than the number of formins on the bead estimated experimentally, and plateaus for beads with more than ~100 formins. This discrepancy can be partly explained by the fact that not all the adsorbed formins are functional. This argument can also explain the large variability in the number of filaments nucleated by a bead (Fig. 4D). In addition, as we show below, the number of filaments attached to the bead is limited by mechanical stress applied by elongating filaments on the formins. Overall, the variability in the number of filaments in bundles likely explains the diversity of bead trajectories or loops observed in the same experimental conditions (Figs. 1A and 4A).

In addition to the persistence length, our model also allowed us to determine the magnitude of the depletion forces that keep the loop stems together. Indeed our model predicts that the self-interacting force density k_S is attractive along the stem up to the junction between loop and stem sections (red arrows, Figs. 3G and 3H). For single filaments, it peaks ~100 pN.µm^{-1} at the transition between the stem and the loop, where elastic forces from the loop counterpoise attraction in the stem (Fig. 3G and 3H). The forces we measured are larger than the forces that were estimated in previous experiments (40) but this difference could be explained by the nature and concentrations of the crowding agents used in each experiment being largely different (0.2% methylcellulose vs ~2% PEG). In addition, our model evaluates the force at each point along the filament, whereas the model in (40) only considered a point force where the loop closes.

Bead stalling as a transition between polymerization-dominated to elasticity-dominated regimes

To test whether the difference in the mechanical properties of the bundle can explain our experimental results, we developed a model for bundle mechanics and bead movement (Fig. 1B), where the bundle is modeled as a single elastic rod with bending rigidity L_P and contour length L *(Appendix A and B)*. The bundle elongates from its barbed end which is attached to the bead via formins. We assume that the bead-filament attachment remains unchanged during the whole process. In particular, the formin-bead or formin-filament link does not break, whatever the magnitude of the force developed by the filament polymerization. The other end of the bundle is assumed to have a fixed position and orientation on the coverslip, as experimentally observed. The transition between bead movement and bundle deformation depends on the balance between two antagonistic forces, namely 1) the force produced by actin polymerization and 2) the viscous drag due to the viscosity of the medium on the bead (Fig. 5A). The physical origin of these forces and their order of magnitude are given in Table 2. If the force required to deform a bundle is higher than the drag force, the bead is steadily pushed forward while the bundle remains straight (Fig.5A, left). Conversely, when the viscous drag is larger than the critical buckling force of the bundle, the bead stalls, and the force generated by the elongation deforms the bundle (Fig. 5A, right). This critical buckling force scales as the reciprocal of the square bundle length (adapted from equation A.13)

$$F_{Buckling} = \gamma \frac{(kT)\pi^2 L_{p0} N^{3/2}}{L^2} \qquad Eq.3$$

where L_P is the persistence length of a single actin filament, N is the number of filaments in the bundle, L is the bundle length, and γ is a numerical factor that depends on the boundary conditions at the bundle ends; here β=1 (filaments free to slide in the bundle).

Therefore, in conditions of constant elongation, the bundle length will eventually meet the condition for buckling, and the exact time for this transition to occur depends on the bundle rigidity or, equivalently, the number of filaments in the bundle (Eq. A15).

In the analysis presented so far, we simplified the transition phase and we did not include the drag force applied to the bundle itself. The transition phase is complex, since within a very short period of time, the bead velocity drops from a constant value to zero while the bundle starts deforming and its transversal movement drags fluid around it. In principle, we cannot rule out post-buckling micro-movement of the bead. However, our experimental data show that this period is extremely short (less than one second) and abrupt (Fig. 2). The bead stalls almost suddenly and, simultaneously, the bundle starts deforming upon actin polymerization.

Our mathematical model for bead movement (equations B.1 to B.5) reproduces the transitions between both kinds of movement (Figs. 5B, 2A and 2C) and shows the dependence of this transition on bundle rigidity L_P. Bundles with relatively low persistence lengths (e.g. L_p=50μm) cannot propel the bead throughout the medium over a long period of time (Fig. 5B). Once the critical buckling condition is reached, i.e. when the bundle reaches the critical length), $L_{Crit} = \sqrt{\left(\frac{\gamma\pi^2(kT)L_{P0}}{F_{Drag}}\right)N^{3/2}}$(adapted from equation A.15 with β=1, as in the case of sliding filaments), the bead stops while the bundle continues its growth. This situation is persistent over time, since the elastic force produced by the bent bundle diminishes with the bundle length as

$$F_{Buckling} = \frac{K}{L^2}, \quad \text{Eq. 4}$$

where K is a constant (equation A.13). In the case of high bundle rigidity (e.g L_p=150μm), the bundle remains straight for about one hour during which the bead moves at a constant velocity without bending the bundle (Figs. 5B and 2D). The shape of the bundle when the bead is stalled (Fig. 5B) is in very good agreement with experimental data (Fig 1A). Presently, in absence of available experimental data, we weren't able to test whether thicker bundles, made of several filaments, would buckle at longer length than bundles made of few (less than 5) filaments.

The expression for L_{Crit} also allowed us to draw a boundary between bead motility and bundle deformation (Fig. 5C). During a typical experiment, the persistence length of the bundle for a given bead remains constant while its length increases. Therefore, it is represented by a trajectory along a vertical arrow in the phase diagram (Fig. 5C). The bead starts with a short bundle (under the phase transition boundary), then elongates while pushing the bead forward, until the bundle eventually reaches the critical length. Above this critical value, the bundle bends and the bead stalls (Figs. 1A and 5C, dashed arrow). Increasing viscosity of the medium increases the resistance to movement and shifts the phase transition boundary downwards in the phase space without altering its shape (Fig. 5D, Eq. A15). If polymerization is stopped (by depleting the free actin monomers) and if friction of the bead and/or the bundle against the glass or the fluid is eliminated, the bundle should keep its straight configuration, whatever the bundle thickness or length. This prediction could be tested in future experiments.

DISCUSSION

Buckling as a mechanism to control filopodia length

Our results suggest that formin-driven extension of bundles, similar to the bundles in filopodia, is mainly controlled by bundle rigidity (Fig. 5), which is proportional to the number of active barbed ends. For example, when a filopodia reaches a critical length, which is determined by its filament density and attachment to the plasma membrane via formins and/or Ena/VASP, it stops pushing the membrane and buckles (41, 42). This transition between extension and buckling (Fig. 5, panels C and D) yields a simple and robust way to control the extension of filopodia in cells, as seen *in vivo* (13, 43). This mechanism is also important for the creation and stability of cell-cell junction in cell tissues, particularly in the formation of villi of same size that ensure tissue coherence (13, 14).

Buckling is a way to release elastic energy in networks and accompany cytoskeleton deformation

Both *in vitro* experiments and models have shown the importance of buckling in the contraction of disordered stress fibers (21) and in the final dismantling of the network (20). Our study suggests this principle may be extended to the whole cell itself. When a bundle of filaments is subjected to mechanical forces, from other cells, obstacles or external forces for example, its buckling under a critical load may constitute an initial response that could trigger a more complex signaling pathway in the cell. Then, differences in the bundle composition (e.g. by modulating the nature or amount of crosslinks, motor proteins, number of filaments), geometry (e.g. by modulation bundle length, anchoring at the plasma membrane or on an organelle) and/or mechanics would modulate the cell response and yield different fates for the cell cytoskeleton. When bundles are stiff (e.g. if they are crosslinked or composed of a large number of filaments), the elastic restitution of the energy stored in bundle buckling could allow cells to resist external constraints. For soft bundles (long ones, without crosslinkers or made of severed filaments), the stressed cytoskeleton would fall in rapidly. For example, it has been shown that spatial 3D distribution of bundles and their interactions (either bundle-bundle or bundle-rest of the cytoskeleton junctions) is crucial for cells (44). Last, bundles are part of the fiber system allowing cells to communicate with other cells (e.g. bundles in villi), to sense the extracellular space (e.g. filopodia) or to couple to focal adhesions. Therefore, any biological condition that change either the geometry or the mechanics of bundles could exert control over cell dynamics.

APPENDICES

Appendix A. Simplified model for the analysis of experiments.

Correct interpretation of experimental observations in Fig. 1 requires the determination of actin filament bundle rigidity. We limit our model for bundle mechanics/deformation to 2D-bending strain. This is dictated by the available experimental data (TIRF microcopy images, Fig. 3) which give access to 2D bundle deformation only. Therefore, we assume that bundle rigidity is given by a single parameter, the apparent rigidity modulus (or persistence length) which depends on two quantities: the bending rigidity of a single filament and the number of filaments in a bundle (15). We focus our analysis on bundles which self-interact to form a stem and a loop (Fig. 3). These configurations represent structures at mechanical equilibrium when elastic forces, which tend to straighten the bundle, are balanced by attractive (depletion) forces that bind distant sections of the bundle to form a stem (Fig. 3).

a. *2D equations for mechanical equilibrium of filaments lying in a plane.*

To determine the rigidity of filament bundles (Fig. 1A), we adapt Eqs. 1-2 to two-dimensional (2D) actin filament bundles as observed in TIRF microcopy (Fig. S1B). The material frame vectors $(\mathbf{d}_1, \mathbf{d}_3)$ are in the plane ($\mathbf{d}_2$ points out of the plane). The orientation of the material frame $(\mathbf{d}_1, \mathbf{d}_3)$ requires a single parameter, θ, the angle between $\mathbf{d}_3$ and the horizontal axis. The filament strain or curvature $d\theta/ds$ enters in the definition of bending strain vector as $\kappa = \frac{d\theta}{ds}\mathbf{d}_2$. From Eq. 1, we derive the force and moment balance equation in its component-wise form

$$\begin{aligned} \frac{df_1}{ds} + \frac{d\theta}{ds} f_3 &= f_{ext,1} \\ \frac{df_3}{ds} - \frac{d\theta}{ds} f_1 &= f_{ext,3} \\ C_B \frac{d^2\theta}{ds^2} - f_1 &= 0, \end{aligned} \qquad (A.1)$$

where f_i is the component of the internal force along the director $\mathbf{d}_i$, i=1, 3, and C_B is the bending rigidity. Note that the bending rigidity parameter, C_B, and the persistence length, L_p, are related by $C_B = kTL_p$ where k is the Boltzmann constant and T the temperature in Kelvin. The twist strain, which is proportional to C_T in Eq. 1, is absent in Eq. A.1. This approximation is valid since twist energy is always lower than bending energy (38) and that 2D filament mechanics is controlled by filament bending curvature (24). The inextensibility condition (Eq. 2) gives two equations for the horizontal and vertical components of $\mathbf{r}(s)$:

$$\frac{dx}{ds} = \cos\theta, \quad \frac{dy}{ds} = \sin\theta \qquad (A.2)$$

For filaments or bundles forming a loop (Fig. 3), the right hand side (*rhs)* of Eq. A.1 (two first lines) models the filament-filament interactions responsible for loop formation and its stabilization (Fig. 3A and 3B). Because a loop is symmetric, we assume that the force between

two points on the filament, **M** and **M'**, is directed along the line **MM'** and proportional to $|\mathbf{MM}| = |x|$ (Fig. 3C). The force is attractive as long the points are within a distance r_1 from each other and repulsive if the distance is smaller than r_0 (hard core repulsion). The force vanishes for inter-filament distance x larger than r_1. Using these assumptions, Eqs. A.1 are changed into:

$$\begin{aligned} \frac{df_1}{ds} + \frac{d\theta}{ds} f_3 &= -2k_s \sin\theta \; |x| F(x) \\ \frac{df_3}{ds} - \frac{d\theta}{ds} f_1 &= 2k_s \cos\theta \; |x| F(x) \end{aligned} \qquad (A.3)$$

with

$$F(x) = \begin{cases} -1 & 0 \le x \le r_0 \\ 1 & r_0 \le x \le r_1 \\ \exp(-|x - r_1|/r_2) & r_1 \le x \end{cases} \qquad (A.4)$$

After normalization of the position (*x, y*) and arc length variable *s* by the filament length *L*, the final equations read

$$\begin{aligned} \frac{d\bar{x}}{d\bar{s}} &= \cos\theta \\ \frac{d\bar{y}}{d\bar{s}} &= \sin\theta \\ \frac{d^2\theta}{d\bar{s}^2} &= \alpha_1 n_1 \end{aligned} \qquad (A.5)$$

and

$$\begin{aligned} \frac{dn_1}{d\bar{s}} + \frac{d\theta}{d\bar{s}} n_3 &= -\alpha_2 \sin\theta \; |\bar{x}| F(\bar{x}) \\ \frac{dn_3}{d\bar{s}} - \frac{d\theta}{d\bar{s}} n_1 &= -\alpha_2 \cos\theta \; |\bar{x}| F(\bar{x}) \end{aligned}$$

Where $(\bar{x}, \bar{y}) = (x/L, y/L)$, $\bar{s} = s/L$, $\alpha_1 = (N_0 L^2 / C_B)$ and $\alpha_2 = (2\, k_s L^2 / N_0)$; *L* is the total loop contour length; $N_0 = (kT/L_0)$ is the natural force unit for the system ($\approx 4.1 \times 10^{-15} N$) with L_0=1 μm; n_1 and n_2 are the force components normalized by N_0. Note that α_1 and α_2 are dimensionless parameters. All the variables and parameters are summarized in Table 1. The vertical symmetry of the configuration (Fig. 3C) gives additional relations

$$\begin{aligned} &x(1-s) = -x(s), \quad y(1-s) = y(s), \\ &\theta(1-s) = -\theta(s), \\ &n_1(1-s) = n_1(s), \quad n_3(1-s) = n_3(s), \end{aligned} \qquad (A.6)$$

All these conditions are a direct consequence of the loop symmetry with respect to the vertical *y*-axis.

Variables and parameters used in simulations of bundles.

Variables	Definition	Dimension	Typical value
s	Arc-length	L	20 to 100 µm
(x,y)	Point coordinates on the filament	L	
θ	Angle between the tangent and the horizontal axis		
(f_1, f_3)	Force along $\mathbf{d}_1$ and $\mathbf{d}_3$.	$M.L.T^{-2}$	
Parameters			
kT	Thermal energy	$M.L^2.T^{-2}$	4.1×10^{-21} J
k_S	Self-interaction force density	$M.T^{-2}$	2.7×10^{-3} pN.µm^{-2}
r_1	cut-off distance	L	0.055 µm
r_2	spatial decay for the self-interaction force.	L	0.02 µm

Table 1. Variables and parameters used in the analysis of bundle rigidity.

b. *Boundary conditions.*

The solution of Eqs. (A.5) depends on the boundary conditions at the ends of the filament, i.e., at $\bar{s} = 0$ or $\bar{s} = 1$. Since the attraction force exerted along the stem balances the elastic force due to the loop rigidity (Fig. 3A, 3B and 3C), the components of the internal force (n_1, n_2) should vanish at $\bar{s} = 0$

$$n_1(0) = 0, \quad n_2(0) = 0 \tag{A.7}$$

In consequence, from Eq. A.6, the internal force should also vanishes at $\bar{s} = 1$. We complete the set of boundary conditions by specifying the position of the filament at s=0 and s=1

$$\begin{aligned} \bar{x}(0) = 0, \quad \bar{x}(1) = 0, \\ \bar{y}(0) = 0, \quad \bar{y}(1) = 0. \end{aligned} \tag{A.8}$$

*c. Determination of bundle bending rigidity***.**

The shape of a loop is given by a solution of Eqs. A.5-A.8 which are valid for a 2D-elastic rod. However, since solutions of Eq. A.5 depend on the ratio (α_1/α_2) only, we cannot have access to bundle rigidity directly. Therefore, we first determined the force interaction in the case of a single

filament for which the bending rigidity is known. Then, we used the same method to analyze the elasticity of loops formed by a bundle made of several filaments by scaling the parameters (α_1, α_2) appropriately.

Algorithm for the determination of the interaction parameter in the case of single filament loop (see Table 1).

1. We extracted the configuration of the loop and the stem from the microscopy image (Fig. 3A and 3B) and measured its contour length (L).
2. We normalized the filament configuration and arc-length with the filament contour length L.
3. Using a persistence length of 10 µm for a single actin filament (or a bending modulus $C_B = 4.1 \times 10^{-26} N.m$) (45, 46), and L, we estimated the parameter
4. $\alpha_1 = (N_0 L^2 / C_B)$ (with $N_0 = 4.1 \times 10^{-15} N$)
5. The best configuration fit (Fig. 3E) was obtained by adjusting α_2, the unique free parameter remaining in Eq. A.5.
6. The interactive depletion force k_S was then given by

$$k_s = \frac{1}{2}\frac{\alpha_2}{\alpha_1}\left(\frac{N_0^2}{C_B}\right) \qquad (A.9)$$

Determination of bundle rigidity.

We now focus on the determination of the rigidity of a bundle made of several filaments. Firstly, assuming a close packing of filaments, R, the radius of a bundle made of N filaments, scales as $R/r = \sqrt{N}$, where r is the radius of a single filament (Fig. S2). Secondly, we assume that the interaction force is proportional to the perimeter of the bundle, since we expect that only the filaments in the outer part of the bundle can exert force on filaments outside the bundle (Fig. S2). Therefore, the parameter k_S in Eq. 5 (or α_2 in Eq. A.5) scales as

$$\frac{k_{S,Bundle}}{k_{S,Filament}} = \sqrt{N} \qquad (A.10)$$

In addition, previous studies showed that simple geometrical arguments allow to approximate the apparent bundle rigidity as a power function of the number of filaments

$$\frac{C_{B,Bundle}}{C_{B,Filament}} = N^{\beta} \qquad (A.11)$$

with $1 \leq \beta \leq 2$ (15). The case $\beta=1$ corresponds to filaments free to slide in the bundle, and $\beta=2$ corresponds to totally crosslinked filaments (15). By combining equations A.10 and A.11, we conclude that

$$\left(\frac{\alpha_1}{\alpha_2}\right)_{Bundle} = \frac{1}{N^{1/2+\beta}}\left(\frac{\alpha_1}{\alpha_2}\right)_{Filament} \qquad (A.12)$$

Therefore, by comparing experimental images of bundles forming a loop obtained by TIRFM to a solution of equations A.5-A.12, we can deduce *N*, the number of filament in a bundle, and, thanks to Eq. A.11, the bundle rigidity. Fig. 4A shows typical observed closed loops (dotted lines) and the corresponding optimal solution to Eqs. A.3-A.6 and the parameters listed in Table 1.

c. *Polymerization kinetics and polymerization force.*

In presence of profilin, the polymerization rate for actin filaments barbed ends capped by the processive formin mDia1 is 38 $\mu M^{-1}s^{-1}$ (36). Assuming a depolymerization rate of 0.1 s^{-1} (47), we predict the critical concentration for actin monomer to be $[G]_0$ = 0.037 µM (Table 2). The concentration of actin monomers, which yields a constant elongation of 0.2 $\mu m.min^{-1}$ for actin filaments (measured from Fig. 1 and Fig. 2), is [G]= 0.068 µM (Table 2). In consequence, the maximal force developed by actin polymerization, given by $F_{pol,max} = (kT/\delta)\ln([G]/[G]_0)$, is 0.93 pN (defined in Table 2).

Drag force.
The presence of actin filaments in the bulk increases the apparent viscosity in the experiments close to values characteristic of that of a cell. Direct viscosity measurement *in vivo* reported values ranging from 0.08 to 0.26 Pa.s (48, 49) which represents a hundred-fold increase of viscosity compared to that of water (0.001 Pa.s). Given the polymerization force (0.93 pN) and drag force exerted on a sphere (Table 2), we predict that the drag force during bead movement is in the range 0.01 to 0.032 pN (Table 2).

Buckling force
The critical force required to buckle an elastic bundle is:

$$F_{Buckling} = \gamma \frac{(kT)\pi^2 L_{p0} N^{1/2+\beta}}{L^2}, \qquad (A.13)$$

where L_P is the persistence length of a single actin filament, *N* is the number of filaments in the bundle, *L* is the bundle length, and γ is a numerical factor that depends on the boundary conditions at the bundle ends (7) . In consequence, when the drag force balances the critical force at buckling

$$F_{Buckling} = F_{Drag}, \qquad (A.14)$$

and the bead is stalled while bundle elongation continues. This transition occurs at a critical bundle length given by solving A.14 with the help of A.13

$$\frac{L_{Crit}^2}{N^{1/2+\beta}} = \frac{\gamma \pi^2 (kT) L_{P0}}{F_{Drag}}. \qquad (A.15)$$

Note that the *rhs* of A.15 is a constant which does not depends on bundle characteristics. The estimated values (Table 2) yields critical lengths in the range of experimental observations . From Eq. A.15 and assuming constant elongation, one can predict that large bundles will sustain the bead propagation regime for longer time periods.

Parameter	Definition	Value	Reference
r	Bead radius	2 µm	
C_{B0}	Single actin filament bending rigidity	4.1×10^{-26} N.m	
V_{max}	Constant bead velocity	0.0033 µm.s^{-1}	
k_{on}	Polymerization rate (barbed end) in the presence of formin	38 µM^{-1}.s^{-1}	4
k_{off}	Dissociation rate from the barbed end	1.4 s^{-1}	8
C	Drag coefficient, $C = 6\pi\eta r$	1.13×10^{-7} Pa.s.m	
$[G]_0$	Critical actin monomer concentration (k_{off}/k_{on})	0.037 µM	
[G]	Apparent monomer concentration $[G] = [G]_0 + \frac{V_{max}}{k_{on}\delta}$	0.067 µM	
F_{Pol}	Polymerization force, $F_{pol,max} = (kT/\delta)\ln([G]/[G]_0)$	0.93 pN	
η	Viscosity	0.08 to 0.26 Pa.s	
Estimated drag force	$F_{drag} = (6\pi\eta r)V_{max}$	0.01 to 0.032 pN	
Critical buckling force (*)	$F_{Buckling} = \gamma\frac{(kT)\pi^2 L_{p0}N^{1/2+\beta}}{L^2}$	unknown	
Critical length at buckling (Eq. A. 15)	$\frac{L_{Crit}^2}{N^{1/2+\beta}} = \left(\frac{\gamma\pi^2(kT)L_{P0}}{F_{Drag}}\right)$	40 to 12 µm^2/filament$^{1.5}$ (**)	

(*) N is the number of actin filaments in the bundle; L_{Crit} is the bundle length at the onset of buckling; γ is a numerical factor.

(**) using $\gamma=1$ and $\beta=1$.

Table 2. Kinetic parameters, actin monomer concentration and forces used to model bead displacement.

Appendix B. Model of filament bundles during macroscopic bead movement.

We adapt the set of equations A.5-A.8 to simulate the movement of beads driven by a growing elastic bundle, actin polymerization and the friction that opposes the movement:

$$\begin{aligned} &\frac{df_1}{ds} + \frac{d\theta}{ds} f_3 = 0 \\ &\frac{df_3}{ds} - \frac{d\theta}{ds} f_1 = 0 \\ &C_B \frac{d^2\theta}{ds^2} - f_1 = 0 \end{aligned} \qquad (B.1)$$

The arc-length variable, s, lies in the interval [0, L(t)] where L(t) is the time-dependent bundle length. Assuming that all filaments in the bundle experience the same stress at their barbed end, the global force-dependent elongation rate of the bundle is given by

$$\frac{dL(t)}{dt} = k_{on}([G] - [G]_0) exp\left(-\frac{\Delta E}{kT}\right) \qquad (B.2)$$

In the above equation, k_{on} is the polymerization rate for actin filament capped by formins (36); $[G]$ and $[G]_0$ are, respectively, the concentration of actin monomers and the critical concentration in presence of formin; δ is the radius of a monomer; $\Delta E = \delta|f_3|$ is the work against the elastic force required to insert one monomer between the bead and the barbed end. The final set of equation governs the bead position

$$\begin{aligned} &\frac{dx_B}{dt} = w(t)\cos\theta; \qquad \frac{dy_B}{dt} = w(t)\sin\theta \\ &\text{with} \qquad w(t) = max\left\{0, \quad \left(C\frac{dL(t)}{dt} - F\right)\right\} \end{aligned} \qquad (B.3)$$

where (x_B(t), y_B(t)) is the bead center; θ is the angle between the bundle and the horizontal axis at the junction between the bundle and the bead; F is the magnitude of the constant viscous drag/friction exerted on the bead; C is the coefficient giving the drag exerted on the bead (Table 2).

b. Boundary conditions used to simulate bead movement.

The pointed end (at s=0) remains fixed in time with

$$x(0) = 0, \quad y(0) = 0, \quad \theta(0) = 0 \qquad (B.4)$$

The boundary at s=L(t) connects the bundle and the bead

$$\begin{gathered} x\big(L(t)\big) = x_B(t) - r_B(t)\cos\theta\big(L(t)\big) \\ y\big(L(t)\big) = y_B(t) - r_B(t)\sin\theta\big(L(t)\big) \\ \left(\frac{d\theta}{ds}\right)_{L(t)} = 0 \end{gathered} \qquad (B.5)$$

where r_B is the bead radius.

AUTHOR CONTRIBUTIONS
Designed the research: JLM, LB, JB; performed the experiments: JB, AM, RBP; developed the models: JLM; analyzed the data: JLM, JB; wrote the manuscript: JLM, JB.

ACKNOWLEDGEMENTS
JB was supported in part by the National Institutes of Health/National Institute of General Medical Sciences Grant R01GM115636. LB is supported by an ANR MaxForce (ANR-14-CE11-0012-02).

REFERENCES

1. Vignjevic, D., D. Yarar, M.D. Welch, J. Peloquin, T. Svitkina, and G.G. Borisy. 2003. Formation of filopodia-like bundles in vitro from a dendritic network. J. Cell Biol. 160: 951–962.
2. Pollard, T.D., and J.-Q. Wu. 2010. Understanding cytokinesis: lessons from fission yeast. Nat. Rev. Mol. Cell Biol. 11: 149–155.
3. Goode, B.L., and M.J. Eck. 2007. Mechanism and Function of Formins in the Control of Actin Assembly. Annu. Rev. Biochem. 76: 593–627.
4. Tilney, L.G., M.S. Tilney, and D.J. DeRosier. 1992. Actin filaments, stereocilia, and hair cells: how cells count and measure. Annu. Rev. Cell Biol. 8: 257–74.
5. Moseley, J.B., and B.L. Goode. 2006. The Yeast Actin Cytoskeleton: from Cellular Function to Biochemical Mechanism. Microbiol. Mol. Biol. Rev. 70: 605–645.
6. Kamasaki, T., R. Arai, M. Osumi, and I. Mabuchi. 2005. Directionality of F-actin cables changes during the fission yeast cell cycle. Nat. Cell Biol. 7: 916–917.
7. Lai, F.P.L., M. Szczodrak, J.M. Oelkers, M. Ladwein, F. Acconcia, S. Benesch, S. Auinger, J. Faix, J.V. Small, S. Polo, T.E.B. Stradal, and K. Rottner. 2009. Cortactin promotes migration and platelet-derived growth factor-induced actin reorganization by signaling to Rho-GTPases. Mol. Biol. Cell. 20: 3209–23.
8. Faix, J., D. Breitsprecher, T.E.B. Stradal, and K. Rottner. 2009. Filopodia: Complex models for simple rods. Int. J. Biochem. Cell Biol. 41: 1656–1664.
9. Hotulainen, P., and P. Lappalainen. 2006. Stress fibers are generated by two distinct actin assembly mechanisms in motile cells. J. Cell Biol. 173: 383–94.
10. Yonemura, S. 2011. Cadherin–actin interactions at adherens junctions. Curr. Opin. Cell Biol. 23: 515–522.
11. Haglund, C.M., J.E. Choe, C.T. Skau, D.R. Kovar, and M.D. Welch. 2010. Rickettsia Sca2 is a bacterial formin-like mediator of actin-based motility. Nat. Cell Biol. 12: 1057–1063.
12. Tilney, L.G., P.S. Connelly, L. Ruggiero, K.A. Vranich, G.M. Guild, and D. Derosier. 2004. The role actin filaments play in providing the characteristic curved form of Drosophila bristles. Mol. Biol. Cell. 15: 5481–91.
13. Faix, J., and K. Rottner. 2006. The making of filopodia. Curr. Opin. Cell Biol. 18: 18–25.
14. Mattila, P.K., and P. Lappalainen. 2008. Filopodia: molecular architecture and cellular functions. Nat. Rev. Mol. Cell Biol. 9: 446–454.
15. Mogilner, A., and B. Rubinstein. 2005. The Physics of Filopodial Protrusion. Biophys. J. 89: 782–795.
16. Footer, M.J., J.W.J. Kerssemakers, J.A. Theriot, and M. Dogterom. 2007. Direct measurement of force generation by actin filament polymerization using an optical trap. Proc. Natl. Acad. Sci. 104: 2181–2186.
17. Burridge, K., and E.S. Wittchen. 2013. The tension mounts: stress fibers as force-generating mechanotransducers. J. Cell Biol. 200: 9–19.
18. Gupton, S.L., and C.M. Waterman-Storer. 2006. Spatiotemporal Feedback between Actomyosin and Focal-Adhesion Systems Optimizes Rapid Cell Migration. Cell. 125: 1361–1374.
19. Gardel, M.L., I.C. Schneider, Y. Aratyn-Schaus, and C.M. Waterman. 2010. Mechanical integration of actin and adhesion dynamics in cell migration. Annu. Rev. Cell Dev. Biol. 26: 315–33.
20. Murrell, M.P., and M.L. Gardel. 2012. F-actin buckling coordinates contractility and

severing in a biomimetic actomyosin cortex. Proc. Natl. Acad. Sci. 109: 20820–20825.
21. Lenz, M., M.L. Gardel, and A.R. Dinner. 2012. Requirements for contractility in disordered cytoskeletal bundles. New J. Phys. 14: 033037.
22. Stachowiak, M.R.R., P.M.M. McCall, T. Thoresen, H.E.E. Balcioglu, L. Kasiewicz, M.L.L. Gardel, and B. O'Shaughnessy. 2012. Self-organization of myosin II in reconstituted actomyosin bundles. Biophys. J. 103: 1265–74.
23. Ramachandran, S., and J.-P. Ryckaert. 2013. Compressive force generation by a bundle of living biofilaments. J. Chem. Phys. 139: 064902.
24. Berro, J., A. Michelot, L. Blanchoin, D.R. Kovar, and J.-L. Martiel. 2007. Attachment conditions control actin filament buckling and the production of forces. Biophys. J. 92: 2546–58.
25. Pronk, S., P.L. Geissler, and D.A. Fletcher. 2008. Limits of Filopodium Stability. Phys. Rev. Lett. 100: 258102.
26. Rückerl, F., M. Lenz, T. Betz, J. Manzi, J.-L. Martiel, M. Safouane, R. Paterski-Boujemaa, L. Blanchoin, and C. Sykes. 2017. Adaptive Response of Actin Bundles under Mechanical Stress. Biophys. J. 113: 1072–1079.
27. Bathe, M., C. Heussinger, M.M.A.E. Claessens, A.R. Bausch, and E. Frey. 2008. Cytoskeletal bundle mechanics. Biophys. J. 94: 2955–64.
28. Lenz, M., T. Thoresen, M.L. Gardel, and A.R. Dinner. 2012. Contractile units in disordered actomyosin bundles arise from F-actin buckling. Phys. Rev. Lett. 108: 238107.
29. Zhuravlev, P.I., Y. Lan, M.S. Minakova, and G.A. Papoian. 2012. Theory of active transport in filopodia and stereocilia. Proc. Natl. Acad. Sci. 109: 10849–10854.
30. Ennomani, H., G. Letort, C. Guérin, J.-L. Martiel, W. Cao, F. Nédélec, E.M. De La Cruz, M. Théry, and L. Blanchoin. 2016. Architecture and Connectivity Govern Actin Network Contractility. Curr. Biol. 26: 616–626.
31. Dorn, J.F., L. Zhang, T.-T. Phi, B. Lacroix, P.S. Maddox, J. Liu, and A.S. Maddox. 2016. A theoretical model of cytokinesis implicates feedback between membrane curvature and cytoskeletal organization in asymmetric cytokinetic furrowing. Mol. Biol. Cell. 27: 1286–99.
32. Tang, H., T.C. Bidone, and D. Vavylonis. 2015. Computational model of polarized actin cables and cytokinetic actin ring formation in budding yeast. Cytoskeleton. 72: 517–533.
33. Bidone, T.C., H. Tang, and D. Vavylonis. 2014. Dynamic Network Morphology and Tension Buildup in a 3D Model of Cytokinetic Ring Assembly. Biophys. J. 107: 2618–2628.
34. Stachowiak, M.R., C. Laplante, H.F. Chin, B. Guirao, E. Karatekin, T.D. Pollard, and B. O'Shaughnessy. 2014. Mechanism of cytokinetic contractile ring constriction in fission yeast. Dev. Cell. 29: 547–61.
35. Michelot, A., J. Berro, C. Guérin, R. Boujemaa-Paterski, C.J. Staiger, J.-L. Martiel, and L. Blanchoin. 2007. Actin-filament stochastic dynamics mediated by ADF/cofilin. Curr. Biol. 17: 825–33.
36. Kovar, D.R., E.S. Harris, R. Mahaffy, H.N. Higgs, and T.D. Pollard. 2006. Control of the Assembly of ATP- and ADP-Actin by Formins and Profilin. Cell. 124: 423–435.
37. Michelot, A., E. Derivery, R. Paterski-Boujemaa, C. Guérin, S. Huang, F. Parcy, C.J. Staiger, and L. Blanchoin. 2006. A novel mechanism for the formation of actin-filament bundles by a nonprocessive formin. Curr. Biol. 16: 1924–30.
38. De La Cruz, E.M., J.-L. Martiel, and L. Blanchoin. 2015. Mechanical Heterogeneity Favors Fragmentation of Strained Actin Filaments. Biophys. J. 108: 2270–2281.

39. Romero, S., C. Le Clainche, D. Didry, C. Egile, D. Pantaloni, and M.-F. Carlier. 2004. Formin is a processive motor that requires profilin to accelerate actin assembly and associated ATP hydrolysis. Cell. 119: 419–29.
40. Lau, A.W.C., A. Prasad, and Z. Dogic. 2009. Condensation of isolated semi-flexible filaments driven by depletion interactions. EPL (Europhysics Lett. 87: 48006.
41. Ludueña, M.A., and N.K. Wessells. 1973. Cell locomotion, nerve elongation, and microfilaments. Dev. Biol. 30: 427–440.
42. Argiro, V., M.B. Bunge, and M.I. Johnson. 1985. A quantitative study of growth cone filopodial extension. J. Neurosci. Res. 13: 149–162.
43. Medeiros, N.A., D.T. Burnette, and P. Forscher. 2006. Myosin II functions in actin-bundle turnover in neuronal growth cones. Nat. Cell Biol. 8: 215–26.
44. Kim, D.-H., S.B. Khatau, Y. Feng, S. Walcott, S.X. Sun, G.D. Longmore, and D. Wirtz. 2012. Actin cap associated focal adhesions and their distinct role in cellular mechanosensing. Sci. Rep. 2: 555.
45. Gittes, F., B. Mickey, J. Nettleton, and J. Howard. 1993. Flexural rigidity of microtubules and actin filaments measured from thermal fluctuations in shape. J. Cell Biol. 120: 923–34.
46. Isambert, H., P. Venier, A.C. Maggs, A. Fattoum, R. Kassab, D. Pantaloni, and M.F. Carlier. 1995. Flexibility of actin filaments derived from thermal fluctuations. Effect of bound nucleotide, phalloidin, and muscle regulatory proteins. J. Biol. Chem. 270: 11437–44.
47. Pollard, T.D. 1986. Rate constants for the reactions of ATP- and ADP-actin with the ends of actin filaments. J. Cell Biol. 103: 2747–54.
48. Kuimova, M.K., G. Yahioglu, J.A. Levitt, and K. Suhling. 2008. Molecular Rotor Measures Viscosity of Live Cells via Fluorescence Lifetime Imaging. J. Am. Chem. Soc. 130: 6672–6673.
49. Kuimova, M.K., S.W. Botchway, A.W. Parker, M. Balaz, H.A. Collins, H.L. Anderson, K. Suhling, and P.R. Ogilby. 2009. Imaging intracellular viscosity of a single cell during photoinduced cell death. Nat. Chem. 1: 69–73.

FIGURE LEGENDS

Figure 1. Bead motility mediated by bundles of actin filaments nucleated by processive formins (mDia1). Panel A: Beads coated with formins mDia1 (20 to 160 formins/bead) are added to a F-actin motility medium (8 µM F-actin, 4 µM profilin and 10 µM ADF/cofilin.) Actin filaments are arrayed in parallel bundles with their barbed at the bead surface. In some cases, the force developed by actin polymerization propels the bead at constant velocity (~ 0.25-0.27 $\mu m.min^{-1}$) for up to one hour (bundle and bead at the top). In other cases, the driving force fails to move the bead after a certain time of steady displacement (e.g. 30 min for the bead at the bottom) while polymerization continues, as demonstrated by bundle deformation. Panel B: Schematic of the mechanical model for bead motility and bundle deformations. We combine the mechanics of bundle with elongation at the barbed end. The polymerization rate is corrected by a term depending on ΔE, the mechanical work necessary to insert a monomer.

Figure 2. Bundle elongation and bead displacement kinetics.
Panels A and B: The bundle length (blue dots) and the bead trajectory (red dots) for the two examples shown in Fig. 1A (A: bottom bead; B: top bead). The dashed curves represent linear interpolation of experimental points. Panels C and D: Simulation of the bead displacement and bundle elongation using Eqs. B.1-B.5 for bundles with persistence lengths of 50 µm (C) and 150 µm (D).

Figure 3. Loops formed by individual filaments and bundles of filaments.
Panels A and B: A folded filament forms a flat loop which is stabilized by attractive forces along the stem (dashed green arrow, panel B) balancing the elastic forces along the loop (dashed blue arrow, panel B). Panel C: Geometric model of the filament configuration in panel A. M is a point at distance s from the loop origin O; θ is the angle between the unit vector tangent to the filament at M (black arrow) and the horizontal axis. To simplify the model, we consider that the attraction force exerted on M is horizontal, along the line MM'. M' is the point symmetric to M located at a distance L-s from O. Additionally, we assume that the attraction between M and M' depends on $|MM'|$ only. Panel D: Cartoon showing how attractive forces along the loop stem (blue arrows) balance the elastic forces caused by filament bending (green arrows). Panel C: Superposition of a loop formed by a bundle of filaments and the associated solution from our 2D model. Bar: 5 µm. Panels E and F: Representative loops from a single filament (E) and a bundle (F) can be fitted with our 2D model for elastic filaments (superimposed red line). Scale bars: 5 µm. Panels G and H: The attractive force density can be determined by our model. Panel G: Schematic representation of the magnitude and sign of the the attaction force. Panel H: Distribution of the repulsion/attraction horizontal force as a function of the arc-length position for the solution of the single filament shown in panel E.

Figure 4. Estimation of bundles' persistence length by the fitting of loops
Panel A: Representative bundle loops for different density of formin. The blue curves is the best fit by Eqs. 7-10 (with β=1) to the experimental loops, which are shown in red. Horizontal and vertical axis are in micrometers. Panels B and C: Persistence length of bundles determined using Eqs. 7-10 assuming the filaments are bound together (β=2, panel B) or slide perfectly relatively to each other (β=1, panel C). Each red dot represent the data for one loop and the average and standard deviation are plotted in blue. Panel D: Number of actin filaments in the

bundles estimated from the rigidity measurement assuming perfect sliding in the bundle (β=1, blue dots) or cannot slide (β=2, red dots).

Figure 5. Motility and bundle deformation. Panel A: The unbalance between polymerization and opposing forces (e.g. drag forces) on the bead controls the transition from bead movement to bundle deformation (left: polymerization overcomes the drag and other opposing forces; right: the drag and other forces stall the bead). Panel B: The bundle rigidity controls the transition between bead movement and bundle deformation. Shaded areas give conditions for which bundles generate enough force to propel the bead. Panels C and D: Phase diagrams for bead movement and bundle deformation. Panel C: Transition between bead motility and bundle deformation in the parameter space (bundle length vs bundle rigidity). The dashed and solid arrows illustrates the typical trajectory in the phase diagram space associated with, respectively, a stalling bead (Fig. 1A, bottom, Figs. 2A and 2C) and a moving bead (Fig 1A, top, Figs. 2B and 2D). Panel D: Increasing the viscous drag force controls the position of the transition curve separating motility and bundle deformation.

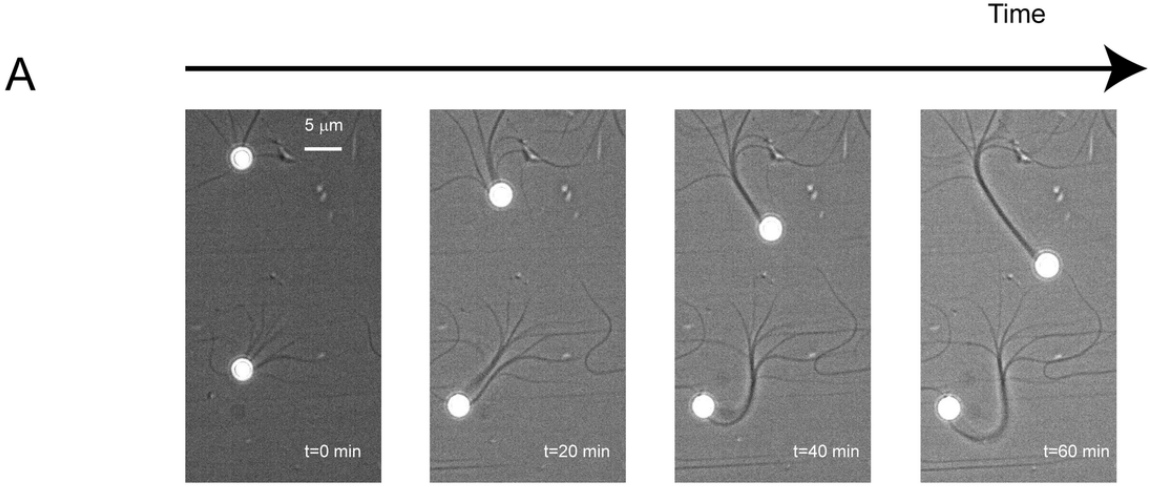

B

Bundle bending

$$E = \left(\frac{C_B}{2}\right)\int_0^L \frac{ds}{R^2(s)}$$

Pointed ends:
-no polymerization/depolymerization

Fixed position

Processive formin / barbed end

-association rate: $k_{on,Barbed}\left([G]-[G]_0\right)\exp\left(-\frac{\Delta E}{kT}\right)$

-dissociation rate: $k_{off,Barbed}$

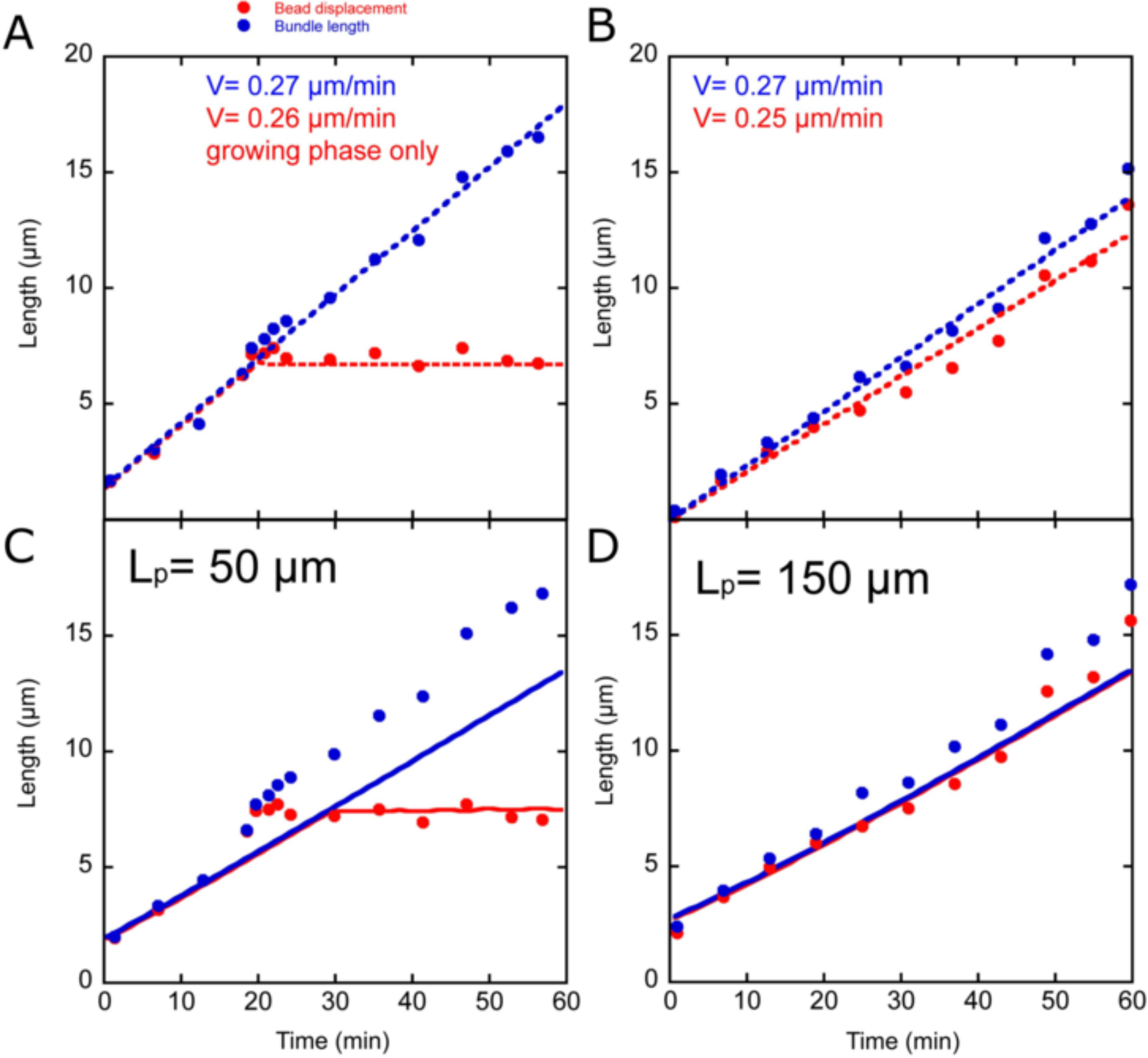
A
B
C
D
Bead displacement
Bundle length
V= 0.27 µm/min
V= 0.26 µm/min
growing phase only
V= 0.27 µm/min
V= 0.25 µm/min
Lp= 50 µm
Lp= 150 µm
Length (µm)
Time (min)
0
5
10
15
20
0
10
20
30
40
50
60

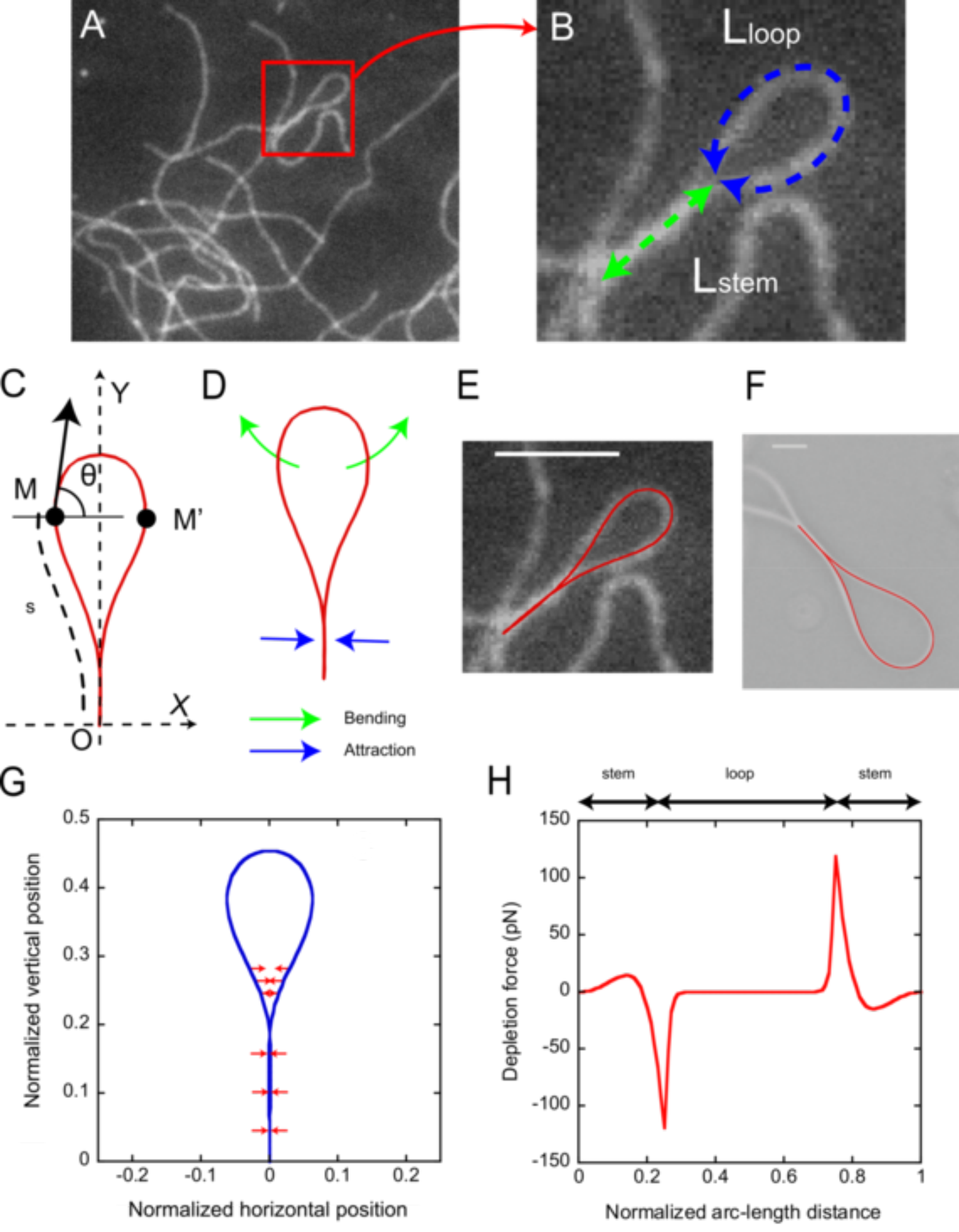
A
B
Lloop
Lstem
C
Y
θ
M
M'
s
X
O
D
Bending
Attraction
E
F
G
Normalized vertical position
Normalized horizontal position
0.5
0.4
0.3
0.2
0.1
0
-0.2
-0.1
0
0.1
0.2
H
stem
loop
stem
Depletion force (pN)
Normalized arc-length distance
150
100
50
0
-50
-100
-150
0
0.2
0.4
0.6
0.8
1

A

[mDia]= 1,000 nM,
160 formins/bead

[mDia]= 750 nM,
120 formins/bead

[mDia]= 500 nM,
80 formins/bead

[mDia]= 250 nM,
40 formins/bead

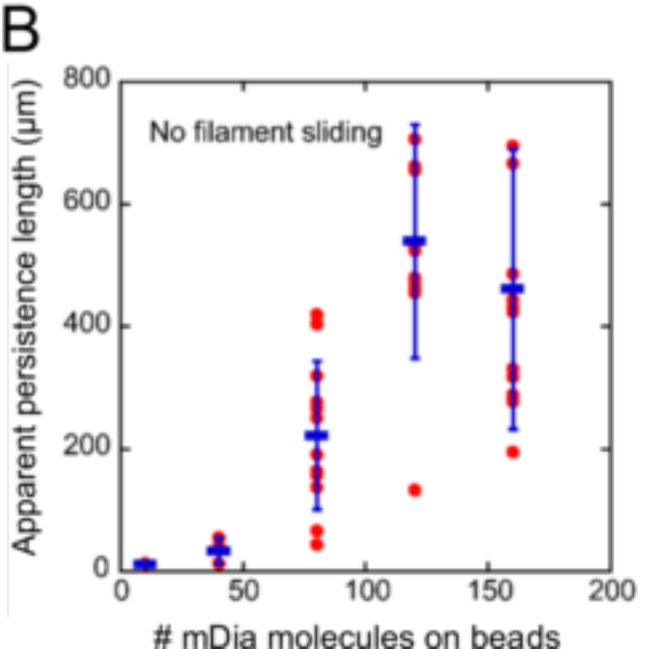

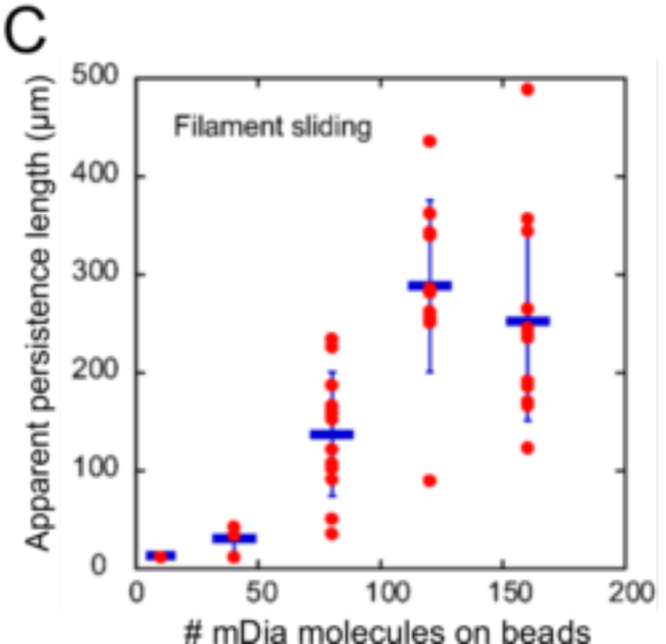

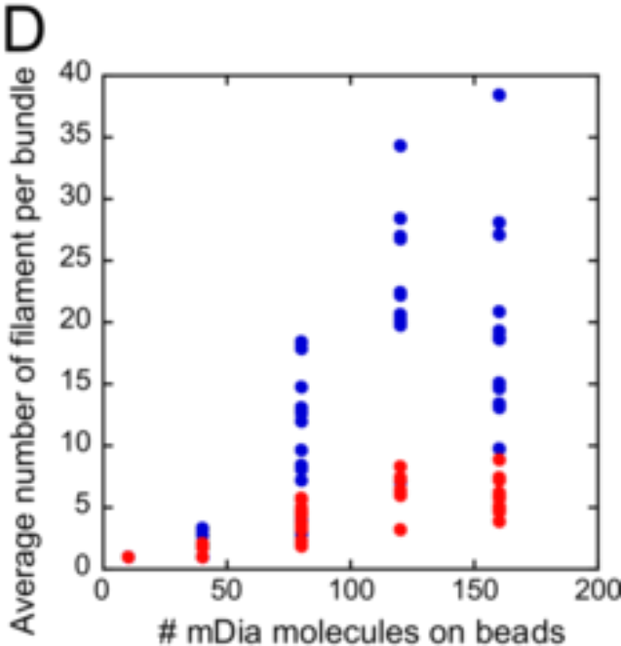

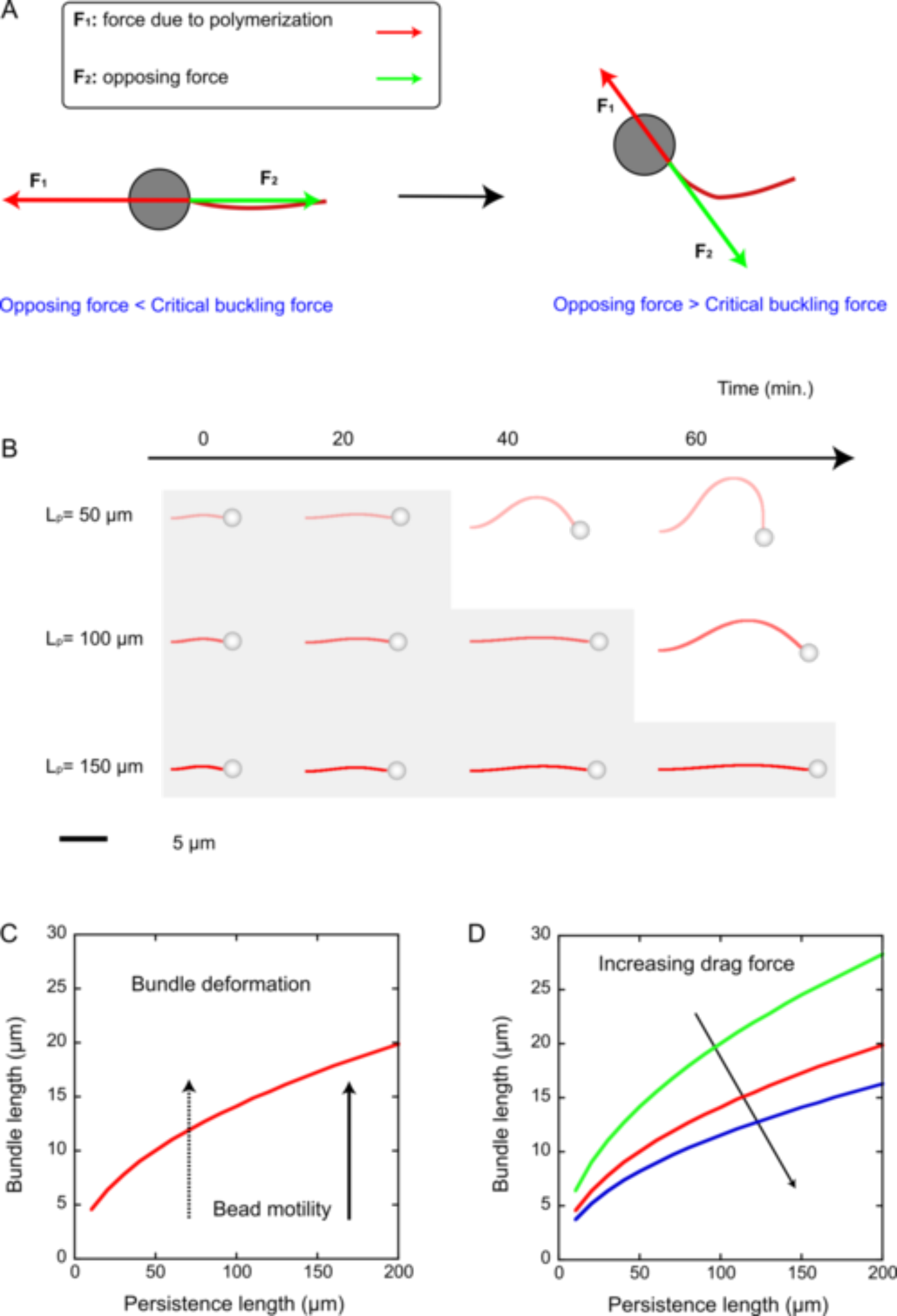
A
F1: force due to polymerization
F2: opposing force
F1
F2
F1
F2
Opposing force < Critical buckling force
Opposing force > Critical buckling force
Time (min.)
B
0
20
40
60
Lp= 50 μm
Lp= 100 μm
Lp= 150 μm
5 μm
C
Bundle deformation
Bead motility
Bundle length (μm)
Persistence length (μm)
0
5
10
15
20
25
30
0
50
100
150
200
D
Increasing drag force
Bundle length (μm)
Persistence length (μm)